PHOTONICS Research

Chirality-selective transparency induced by lattice resonance in bilayer metasurfaces

Shuxia Zhao,[1] Lei Shao,[2] Jianfang Wang,[3] Hai-Qing Lin,[2,4] and Wei Zhang[1,2,5]

[1]Institute of Applied Physics and Computational Mathematics, Beijing 100088, China
[2]Beijing Computational Science Research Center, Beijing 100193, China
[3]Department of Physics, The Chinese University of Hong Kong, Shatin, Hong Kong SAR, China
[4]e-mail: haiqing0@csrc.ac.cn
[5]e-mail: zhang_wei@iapcm.ac.cn

Received 26 November 2020; revised 20 January 2021; accepted 24 January 2021; posted 25 January 2021 (Doc. ID 416015); published 19 March 2021

Chiral optical responses of bilayer metasurfaces made of twisted metallic nanorods are investigated in detail with focus on the collective effect due to lattice resonance (LR). Using an analytical approach based on the coupled dipole method (supported by full wave simulation), we find optical chirality is dramatically increased by the coupling between localized surface plasmon resonances and LR. The collective effect results in significant chiral signal even for metasurfaces made of achiral unit cells. The interlayer coupling generally destroys the Wood's anomaly and the associated transparency. While making use of Pancharatnam–Berry (PB) phase and propagation phase, one can modulate the optical activity effectively and achieve chirality-selective transparency induced by LR in a designed structure with a *g*-factor of absorption as high as 1.99 (close to the upper limit of 2). Our studies not only reveal a new mechanism of modulating chiral optical response by combination effects from PB phase, propagation phase, and LR, but also give a quantitative relationship between the geometry configuration and chiral optical properties, thus providing helpful guidance for device design.

https://doi.org/10.1364/PRJ.416015

1. INTRODUCTION

Chirality is of great importance in fundamental science, material design, biomedicine, and so on. Chiral optics associated with natural chiral molecules is limited by the fixed geometrical structure and weak optical signal mainly in the ultraviolet (UV) range. Plasmonic clusters supporting localized surface plasmon resonances (LSPRs) interact with visible light strongly, which can be controlled by the shape, size, position, and permittivity of the objects [1]. Plasmonic nanostructures can be precisely designed with complex geometric patterns and thus provide many opportunities for exploring light–matter/structure interaction, in particular the chiral nature of photonics. In the past decade, many types of chiral clusters have been explored to study circular dichroism (CD), such as helical particles [2,3], tetramers [4], hybrid L-shaped resonators [5], U-shaped antennas [6,7], hybrid rod-sphere structures [8], various dimers [9–14], and others [15,16]. Using intrinsic chiral clusters as building blocks, chiral metamaterials/metasurfaces [17–23] can discriminate right- and left-circularly polarized (RCP and LCP) light, and they can even realize selective transmission of different circularly polarized light [24–26]. Furthermore, 2D planar metasurfaces with extrinsic chirality can realize asymmetric transmission/reflection [27–30] as well as modulation of light's wavefront, direction, and polarization [31–34], which is promising in developing metalenses. The responses of metasurfaces of stacked layers are discussed in the view of photonic systems [19,20,35,36]. Besides designing nanostructures, a structured light field (superchiral light) [37,38] is proposed to increase light–material interaction, which is promising in amplification of chiral molecules' CD signal [39].

Collective effects {such as lattice resonance (LR) [40–44]} and interference effects (such as Fano resonance [45] and electromagnetic induced transparency) modulated by electromagnetic (EM) field phase play important roles in controlling the optical properties. However, the study of the combination of those effects in the chiral metasurface area is in the preliminary stage [22,46–51]. Many important issues need systematic studies. For example, it is known that the geometric configuration, such as the relative orientation/position of the substructure, affects the collective resonance [43,50,52], phases of the EM field {Pancharatnam–Berry (PB) [31,53,54] and propagation phase}, and mirror symmetry breaking (related to chiral response) [4,14,52]. Much effort is needed to investigate the physical consequence of the interplay of these effects, the resulting (chiral) optical properties, the applications in optics modulation, and device design.

Here we take an archetypical chiroptical nanorod dimer [9,55] as the building block of the metasurfaces to explore the combination effects of collective resonance and interference on the chiral optics. Using an analytical approach based on a coupled dipole model (CDM) and finite-difference time-domain (FDTD) simulation, we find that the optical chirality of the metasurface is dramatically increased by the coupling between LSPRs and LR. The collective effect results in significant chiral signal, even for metasurfaces made of achiral unit cell-orthogonal nanorod dimers. By using phase (PB phase and propagation phase) modulated LR, different chiral responses can be obtained; in particular, chirality-selective transparency [100% transmission and a *g*-factor of absorption up to 1.99 (close to the upper limit of 2)] associated with Wood's anomaly is realized in a specially designed structure, though in general the interlayer coupling destroys the Wood's anomaly. Our studies reveal a new mechanism of tuning the chiral optical properties based on collective effect assisted by phase modulation (PB phase and propagation phase), and the analytical results (verified by numerical simulation) clearly reveal the quantitative relationship between the geometry configuration and chiral optical responses, providing modern photonic applications such as circular polarizers, optical communication, and quantum information processing.

The paper is organized as follows. First we introduce the analytical formula to calculate the transmittance of metasurfaces. Second, we discuss the chirality of twisted nanorods and LR in monolayer metasurfaces. Third, bilayer metasurfaces' extraordinary chiral transmission induced by LR is discussed and the general relationship between geometry and chiral optical response is given. Finally, we discuss the extraordinary chiral transmission of cases with higher-order resonance, square lattices, and the optical activity beyond the coupled dipole limit.

2. THEORETICAL FORMULA

A. Coupled Dipole Model

The metasurface is constituted by bilayer twisted silver nanorods as shown in Fig. 1. The lattice constants in the x and y directions are Λ_x and Λ_y. Here we use the general terminology of metasurfaces without limitation of the lattice constant. In each unit cell, θ and ϕ are the rotation angles (with respect to the x axis) of the long axis of the nanorods in the upper layer and lower layer, and z_0 is the gap between the two layers.

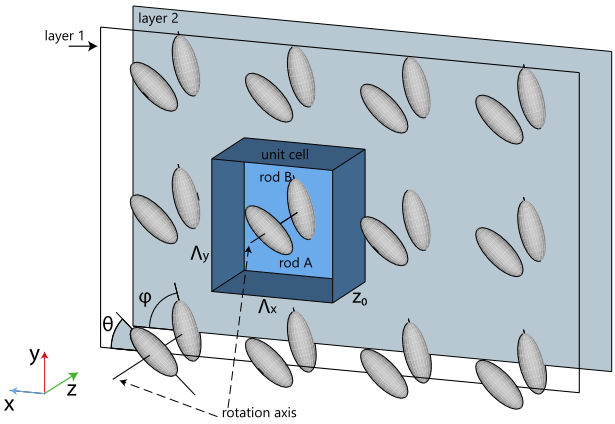

Fig. 1. Scheme of the metasurface made of arrays of twisted nanorod dimers.

For simplicity, the silver nanorods are modeled as ellipsoids, whose long- and short-axis radii are 80 and 30 nm. The longitudinal and transverse LSPRs' resonance wavelengths are at 590 and 355 nm. In the wavelength range 450–700 nm, the dominant mode is due to longitudinal LSPR. Thus, the component of the dipole polarizability tensor along the long axis of the nanorod is considered. Higher-order multipole modes and transverse dipole modes are neglected. Furthermore, the distance between two rods in the nearby/same unit cell is 3 times larger than the long/short axis radius. As a result, the CDM [1,56] is used to describe the interaction between the nanorods:

$$\frac{1}{\alpha}\mathbf{P}_n^A = \hat{F}_A \cdot \left(\mathbf{E}_n^A + \sum_{m\neq n}\hat{G}_{nm}^{AA}\mathbf{P}_m^A + \sum_m \hat{G}_{nm}^{AB}\mathbf{P}_m^B\right),$$
$$\frac{1}{\alpha}\mathbf{P}_n^B = \hat{F}_B \cdot \left(\mathbf{E}_n^B + \sum_{m\neq n}\hat{G}_{nm}^{BB}\mathbf{P}_m^B + \sum_m \hat{G}_{nm}^{BA}\mathbf{P}_m^A\right), \quad (1)$$

where $\mathbf{P}_n^{A/B}$ and $\mathbf{E}_n^{A/B}$ are the induced electric dipole moments and incident electric field at the position of $\mathbf{r}_n^{A/B} = (n_x\Lambda_x, n_y\Lambda_y, 0/z_0)$, n_x and n_y are integers, and A and B represent the upper and lower layer. $\hat{F}_{A/B} \equiv \mathbf{P}_n^{A/B}\mathbf{P}_n^{A/B}/|\mathbf{P}_n^{A/B}|^2$ is the projection tensor. $\hat{G}_{nm}^{AA} = \hat{G}(|\mathbf{r}_n^A - \mathbf{r}_m^A|)$, and the Green's tensor is

$$\hat{G}(r) = (k^2\hat{U} + \vec{\nabla}\vec{\nabla})\frac{e^{ikr}}{4\pi r}, \quad (2)$$

where k is the light momentum in free space and $\hat{U}$ is the 3×3 unit tensor.

The optical response of each nanorod can be described by the polarizability using either an analytical [57] or semi-analytical [58] method. Here we directly use the multipole decomposition method [59–61] to give a precise description. This method is promising for describing nanoparticles with arbitrary shape and size. The dipole polarizability can be obtained as D/E, where E is the electric field along the long axis of the nanorod and D is the total electric dipole moment calculated by the FDTD method (see subsection 2.B on FDTD simulation). The multipole decomposition analysis indicates that the total response of each nanorod is dominated by the total electric dipole moment, and higher multipoles are negligible.

Because of the periodicity in the x–y plane of the metasurface, the Bloch theorem guarantees the solution of Eq. (1) must have the form $\mathbf{P}_n^{A/B} = \mathbf{P}^{A/B}\exp(i\mathbf{k}_{||}\mathbf{r}_{||}^n)$ and the incident electric field $\mathbf{E}_n^{A/B} = \mathbf{E}^{A/B}\exp(i\mathbf{k}_{||}\mathbf{r}_{||}^n)$, including a phase factor involving the incident light's momentum component $\mathbf{k}_{||}$ parallel to a 2D metasurface. Specifically, $\mathbf{k}_{||}$ is zero for normal incident light, i.e., $\mathbf{E}_n^{A/B} = \mathbf{E}^{A/B} = \mathbf{E}_0\exp(ikz^{A/B})$, where $\mathbf{E}_0$ is the electric field amplitude vector. We consider two cases of $(\mathbf{P}^A, \mathbf{P}^B)_{L/R}$ for left-/right-circularly polarized (LCP/RCP) light with electric amplitude vector $\mathbf{E}_{0;L/R} = [\frac{1}{\sqrt{2}}, \frac{\pm i}{\sqrt{2}}, 0]E_0$. After some calculation, we have

$$\mathbf{P}^{A}_{L/R} = \frac{\sqrt{2}}{2}\frac{e^{i(kz_0\pm\phi)}H_{12} + e^{\pm i\theta}H(\phi)}{H(\theta)H(\phi) - H_{12}^2}E_0\hat{e}_A,$$
$$\mathbf{P}^{B}_{L/R} = \frac{\sqrt{2}}{2}\frac{e^{\pm i\theta}H_{12} + e^{i(kz_0\pm\phi)}H(\theta)}{H(\theta)H(\phi) - H_{12}^2}E_0\hat{e}_B, \tag{3}$$

where $\hat{e}_{A/B}$ is the unit vector along the long axis of the nanorod in the upper (A) layer and lower (B) layer. $H_{12} = \hat{\mathcal{G}}^{\mathrm{AB}}_{\mathrm{xx}}\cos\theta\cos\phi + \hat{\mathcal{G}}^{\mathrm{AB}}_{\mathrm{yy}}\sin\theta\sin\phi$, $H(\theta) = \frac{1}{\alpha} - (\hat{\mathcal{G}}^{AA}_{xx}\cos^2\theta + \hat{\mathcal{G}}^{AA}_{yy}\sin^2\theta)$, and $\hat{\mathcal{G}}^{AA} = \hat{\mathcal{G}}^{BB} = \sum_{m\neq 0}\hat{G}^{AA}_{mn}$ is the interaction tensor for nanorods in the same layer. $\hat{\mathcal{G}}^{AB} = \hat{\mathcal{G}}^{BA} = \sum_m \hat{G}^{AB}_{mn}$ describes the interaction of nanorods in different layers. With the help of the Weyl identity

$$\frac{e^{ikr}}{r} = \frac{i}{2\pi}\iint\frac{1}{k_z^q}e^{i(\mathbf{q}_{||}\mathbf{r}_{||} + k_z^q|z|)}\mathrm{d}\mathbf{q}_{||}, \tag{4}$$

with $k_z^q = \sqrt{k^2 - \mathbf{q}_{||}^2}$, and $\mathbf{q} = (\mathbf{q}_{||}, k_z^q)$ an arbitrary 3D vector in k-space, we obtain the interaction tensor as

$$\hat{\mathcal{G}} = \sum_{j=0}^{\infty}\hat{G}(\mathbf{r} - \mathbf{r}_j)$$
$$= \frac{i}{8\pi^2}\sum_{j=0}^{\infty}\int\frac{k^2\hat{U} - \mathbf{qq}}{k_z^q}e^{i[\mathbf{q}_{||}(\mathbf{r}_{||} - \mathbf{r}_{||}^j) + k_z^q|z - z^j|]}\mathrm{d}\mathbf{q}_{||}, \tag{5}$$

where $\mathbf{r}$ is the observation point. Using the relationship

$$\sum_{j=0}^{\infty}e^{i\mathbf{q}_{||}\mathbf{r}_{||}^j} = \frac{(2\pi)^2}{A}\sum_{\mathbf{L}}^{\infty}\delta(\mathbf{q}_{||} - \mathbf{L}), \tag{6}$$

with A the area of lattice unit cell and $\mathbf{L}$ the 2D reciprocal-lattice vectors, the sum of Green's functions in Eq. (3) can be written as

$$\hat{\mathcal{G}}^{AA} = \lim_{z\to 0}\left(\frac{i}{2A}\sum_{\mathbf{L}}^{\infty}\frac{k^2\hat{U} - \mathcal{LL}}{k_z^l}e^{ik_z^l|z|}\right.$$
$$\left. - \frac{i}{2\pi}\int\frac{k^2\hat{U} - \mathbf{qq}}{k_z^q}e^{ik_z^q|z|}\mathrm{d}\mathbf{q}_{||}\right),$$
$$\hat{\mathcal{G}}^{AB} = \frac{i}{2A}\sum_{\mathbf{L}}^{\infty}\frac{k^2\hat{U} - \mathcal{LL}}{k_z^l}e^{ik_z^l|z_0|}, \tag{7}$$

where $k_z^l = \sqrt{k^2 - \mathbf{L}^2}$ and $\mathcal{L} = (\mathbf{L}, k_z^l)$ is a 3D vector. Then we get the conditions to make $\hat{\mathcal{G}}$ divergent, namely, $k = |\mathbf{L}|$. Furthermore, the Green's function of the far field ($\mathbf{r}^{\mathrm{far}}$) due to those dipoles is

$$\hat{\mathcal{G}}^{\mathrm{far}} = \frac{i}{2A}\sum_{\mathbf{L}}^{\infty}\frac{k^2\hat{U} - \mathcal{LL}}{k_z^l}e^{-i\mathbf{L}\mathbf{r}_{\|} + ik_z^l|z - z^j|}. \tag{8}$$

If the wavelength is larger than the lattice constant ($k < \min\{L_x, L_y\}$), then all terms of the sums are evanescent, except that for the $\mathbf{L}_{(0,0)} = (L_x = 0\frac{2\pi}{\Lambda_x}, L_y = 0\frac{2\pi}{\Lambda_y})$, representing the electromagnetic wave propagating in the z direction. If $k > \min\{L_x, L_y\}$, the transmission has higher-order (m, n) grating modes, whose directions are the same as $\mathcal{L}_{(m,n)} = (m\frac{2\pi}{\Lambda_x}, n\frac{2\pi}{\Lambda_y}, k_z^l)$. Finally, the far field of the (0,0) order grating mode [$\mathbf{r}^{\mathrm{far}} = (0,0,z)$ and $z > z_0$] is

$$\mathbf{E}^{A/B}_{(0,0)} = \sum_{j=0}^{\infty}G(\mathbf{r}^{\mathrm{far}} - \mathbf{r}_j^{A/B})\mathbf{P}_j^{A/B} = \hat{\mathcal{G}}^{\mathrm{far}}_{(0,0);A/B}\mathbf{P}^{A/B}$$
$$= \frac{ik}{2A}e^{ik(z - z^{A/B})}\mathbf{P}^{A/B}. \tag{9}$$

After solving the electric field, we can calculate the (0, 0) order transmittance as

$$T_{(0,0)} = \frac{P_{(0,0)}}{P_{\mathrm{inc}}} = \frac{|\mathbf{E}_0e^{ikz} + \mathbf{E}^A_{(0,0)} + \mathbf{E}^B_{(0,0)}|^2}{|\mathbf{E}_0e^{ikz}|^2}$$
$$= 1 - \frac{\sigma}{A} + \frac{k^2}{4A^2|E_0|^2}|\mathbf{P}^A + e^{-ikz_0}\mathbf{P}^B|^2. \tag{10}$$

Note that the extinction cross section (σ) in each unit cell is of the form

$$\sigma = \frac{k}{|E_0|^2}\mathrm{Im}(\mathbf{E}_0^{A*}\mathbf{P}^A + \mathbf{E}_0^{B*}\mathbf{P}^B). \tag{11}$$

Similarly, the reflectance can be calculated as

$$R_{(0,0)} = \frac{P^{(R)}_{(0,0)}}{P_{\mathrm{inc}}} = \frac{|\mathbf{E}^A_{(0,0)} + \mathbf{E}^B_{(0,0)}|^2}{|\mathbf{E}_0e^{ikz}|^2}$$
$$= \frac{k^2}{4A^2|E_0|^2}|\mathbf{P}^A + e^{ikz_0}\mathbf{P}^B|^2. \tag{12}$$

The absorption of the metasurface is defined as $\mathrm{Ab} = 1 - T - R$. Then the absorption g-factor $g = 2(\mathrm{Ab}_L - \mathrm{Ab}_R)/(\mathrm{Ab}_L + \mathrm{Ab}_R)$, and $\mathrm{Ab}_{L/R}$ is the absorption in the presence of LCP/RCP. The analytical approach based on the CDM gives a clear physical picture, and the quantitative results are supported by the FDTD simulation as seen below.

B. FDTD Simulation

In FDTD simulation, the circularly polarized light is generated by the x- and y-direction polarized plane waves with $\pm\pi/2$ phase difference. For a nanorod dimer, perfectly match layer (PML) boundary conditions are used in all boundaries of three dimensions. For metasurfaces, the PML boundary conditions are used in the z direction, while periodic conditions are used in the x and y directions. The mesh cell is cube with size of 4 nm, and silver's refractive index in the visible light range is obtained from Ref. [62].

To calculate the polarizability (α) of one single rod used in CDM, we use the multipole decomposition method [59–61] based on FDTD simulation of one rod:

$$\mathbf{p} = \int\mathbf{P}(\mathbf{r}')\mathrm{d}\mathbf{r}', \tag{13}$$

$$\mathbf{m} = -\frac{i\omega}{2}\int[\mathbf{r}'\times\mathbf{P}(\mathbf{r}')]\mathrm{d}\mathbf{r}', \tag{14}$$

$$\mathbf{T} = \frac{i\omega}{10}\int\{2\mathbf{r}'^2\mathbf{P}(\mathbf{r}') - [\mathbf{r}'\cdot\mathbf{P}(\mathbf{r}')]\mathbf{r}'\}\mathrm{d}\mathbf{r}', \tag{15}$$

for electric, magnetic, and toroidal dipole moments, where $\mathbf{r}'$ belongs to the total ellipsoid. $\mathbf{P}(\mathbf{r}') = [\epsilon(\mathbf{r}') - \epsilon_0]\mathbf{E}(\mathbf{r}')$, where $\mathbf{E}(\mathbf{r}')$ can be directly obtained from the FDTD method. The total electric dipole moment used in this paper is

$$\mathbf{D} = \mathbf{p} + \frac{ik}{c}\mathbf{T}, \tag{16}$$

with c the velocity of light. The polarizability is calculated as $\alpha = D/E$, where D and E are the complex amplitudes of the dipole moment and incident electric field in the long-axis direction.

3. RESULTS AND DISCUSSIONS

A. Optical Responses of a Single Nanorod Dimer and a Monolayer Metasurface: Localized Surface Plasmon Resonance and Lattice Resonance

First we consider a single silver nanorod dimer—the building block of the metasurface. It is known that a nanorod dimer with twisted angle $\theta - \phi = 0$ or $\pi/2$ shows no difference of extinction cross sections for LCP/RCP light incident in the direction of the rotation axis of the dimer due to mirror symmetry [52,55]. The extinction cross sections of a dimer with twisted angle ($\theta - \phi = \pi/4$) are shown in Fig. 2. Resonant peaks appear at 595/605 nm for RCP/LCP light, which manifest the intrinsic chirality of the nanorod dimer. The very good agreement between the results of the full wave simulation based on the FDTD method [Fig. 2 (dash lines)] and those of the CDM [Fig. 2 (solid lines)] indicates the validity of the CDM. Our analytical theory based on CDM includes nonperturbative (higher order of interparticle interaction) effects. To the leading order of interparticle interaction and for $kz_0 \ll 1$, the chiral optical response can be described by rotation strength in terms of effective electric dipole moment and magnetic dipole moment (which can be obtained by multipole decomposition), pointing out the combined role of electric and magnetic dipole moments in chiral optical response, like that for molecular optical activity.

For comparison with new features of chiral optics due to LR in bilayer metasurfaces, we discuss the optical response of a monolayer metasurface made of silver nanorods with a rotational angle θ with respect to the x axis. The CDM gives

$$\frac{1}{\alpha}\mathbf{P}_n^A = \hat{F}_A \cdot \left(\mathbf{E}_n^A + \sum_{m\neq n} \hat{G}_{nm}^{AA}\mathbf{P}_m^A\right). \tag{17}$$

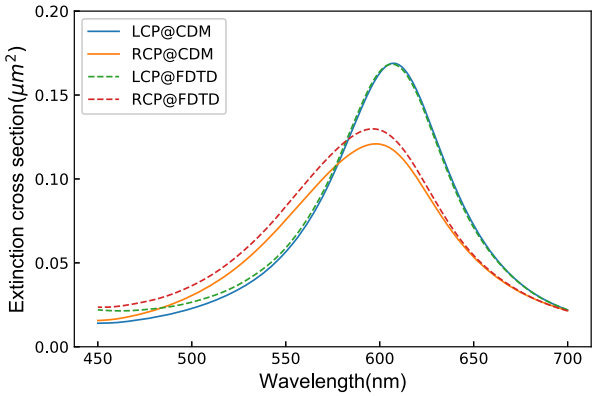

Fig. 2. Extinction cross sections of a dimer with twist angle $\pi/4$ and separation $z_0 = 200$ nm for LCP and RCP light. Solid/dashed lines are the results calculated by CDM/FDTD.

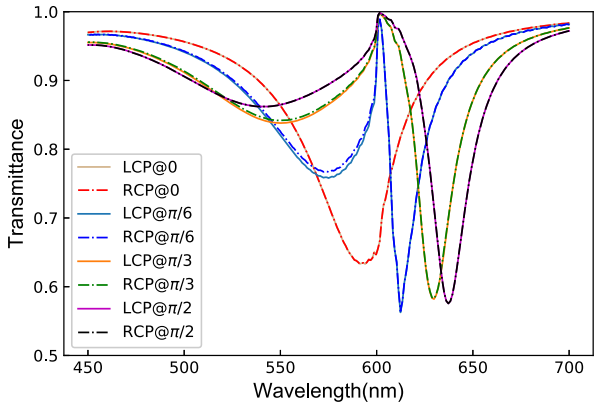

Fig. 3. Transmittances of monolayer metasurfaces with $\theta = 0, \pi/6, \pi/3, \pi/2$ for LCP and RCP light.

In the presence of normally incident LCP/RCP light, the effective dipole moment is

$$\mathbf{P}_{L/R} = \frac{\sqrt{2}e^{\pm i\theta}}{2H(\theta)} E_0(\cos\theta\hat{e}_x + \sin\theta\hat{e}_y). \tag{18}$$

Since the longitudinal LSPR of the nanorod is at 590 nm, we choose $\Lambda_x = 600$ nm and $\Lambda_y = 400$ nm for an effective coupling between LSPR and LR. By combining with Eq. (10), it is easy to see that the transmittances of LCP and RCP light are the same, as expected from the symmetry consideration. As shown in Fig. 3, the typical Wood's anomaly line shape due to LR [63] and transparency (100% transmission) appears at a wavelength of 600 nm (except the case of $\theta = 0$). The phenomenon can be explained by Eq. (18). When $\lambda = \Lambda_x$ ($k = |\mathbf{L}_{(\pm1,0)}|$), $\hat{\mathcal{G}}_{xx}^{AA}$ is convergent and $\hat{\mathcal{G}}_{yy}^{AA}$ is divergent in the denominator. So as long as $\sin^2\theta \neq 0$, $P_{L/R} = 0$ and transmittance is 100% at 600 nm. As the wavelength moves away from 600 nm, two dips in the curve of transmittance may appear under the condition $\mathrm{Re}\{1/\alpha - \hat{\mathcal{G}}_{xx}^{AA}\cos^2\theta - \hat{\mathcal{G}}_{yy}^{AA}\sin^2\theta\} = 0$. When $\theta = 0$, the divergent term $\hat{\mathcal{G}}_{yy}^{AA}$ disappears, so the transparency disappears.

B. Chiral Optical Response of Bilayer Metasurface: The Combination Effects from Lattice Resonance, PB Phase, and Propagation Phase

1. Chirality-Selective Transparency

As for bilayer metasurfaces, nanorods on the two layers may have different rotation angles θ and ϕ. So metasurface's intrinsic chirality leads to different transmission for LCP and RCP light. The transmittances of a typical bilayer metasurface are displayed in Figs. 4(a) and 4(c) for those from FDTD simulation and CDM calculation. Different responses to LCP and RCP light are clearly seen, and there is very good agreement between the results from FDTD simulation and those based on CDM. Interestingly, a quite different response can be found as shown in Figs. 4(b) and 4(d) (for FDTD and CDM). Here one sees chirality-selective transparency. To understand the physics involved, it is helpful to rewrite Eq. (3) in the basis suitable for circularly polarized light. Then one has

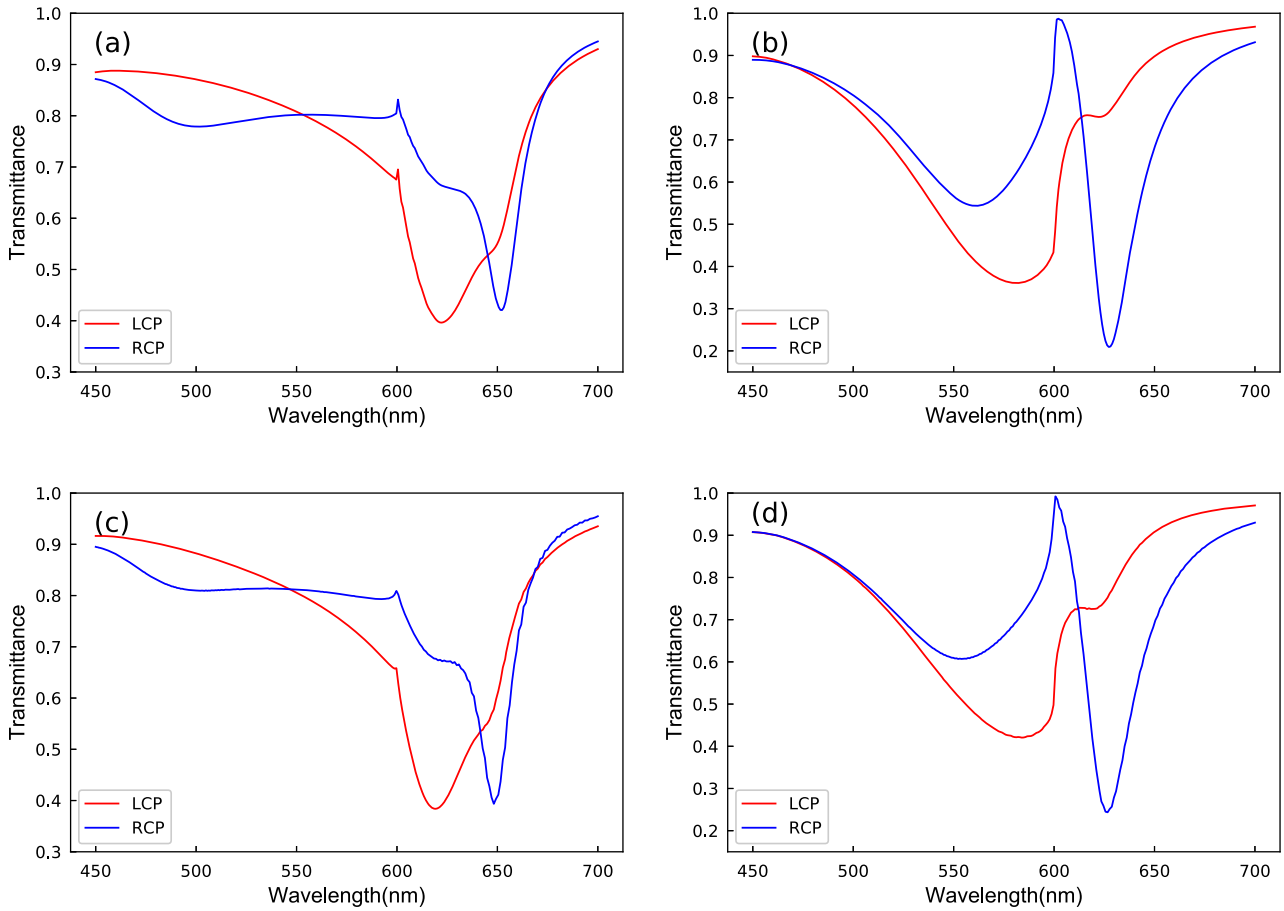

Fig. 4. Transmittance of a bilayer metasurface with parameters $z_0 = 200$ nm, $\Lambda_x = 600$ nm, $\Lambda_y = 300$ nm. (a), (c) $\theta = \pi/3$ and $\phi = \pi/2$; (b), (d) $\theta = \pi/6$ and $\phi = 5\pi/6$. (a), (b) Results based on FDTD simulation; (c), (d) those based on the CDM.

$$\mathbf{P}^A_{L/R} = \frac{E_0}{2\Delta(\theta,\phi)}\{[e^{i(kz_0 \pm \phi - \theta)}H_{12} + e^{i(\pm\theta-\theta)}H(\phi)]\hat{e}_L + [e^{i(kz_0 \pm \phi + \theta)}H_{12} + e^{i(\pm\theta+\theta)}H(\phi)]\hat{e}_R\},$$
$$\mathbf{P}^B_{L/R} = \frac{E_0}{2\Delta(\theta,\phi)}\{[e^{i(\pm\theta-\phi)}H_{12} + e^{i(kz_0 \pm \phi-\phi)}H(\theta)]\hat{e}_L + [e^{i(\pm\theta+\phi)}H_{12} + e^{i(kz_0 \pm \phi+\phi)}H(\theta)]\hat{e}_R\}, \quad (19)$$

where $\Delta(\theta,\phi) \equiv H(\theta)H(\phi) - H^2_{12}(\theta,\phi)$ and $\hat{e}_{L/R} = \frac{\sqrt{2}}{2}(\hat{e}_x \pm i\hat{e}_y)$. In our modulation of optics by metasurfaces, two important factors are phase and LR. We first take a close look at various phases in the above equations. We take

$$\mathbf{P}^B_R = \frac{E_0}{2\Delta(\theta,\phi)}\{[e^{-i(\theta+\phi)}H_{12} + e^{i(kz_0-2\phi)}H(\theta)]\hat{e}_L + [e^{i(\phi-\theta)}H_{12} + e^{ikz_0}H(\theta)]\hat{e}_R]\} \quad (20)$$

as an example to explain the origin of the phases. Obviously, kz_0 is the propagation phase for nanorod B. For normal incidence, there is additional PB phase -2ϕ for the left-circular component (in the second term). The term proportional to H_{12} is due to the interaction from nanorod A. Transforming from coordinates associated with nanorod A to those of B leads to a phase of $\phi - \theta$ (in the third term). Also additional PB phase -2ϕ for the left-circular component leads to $\phi - \theta - 2\phi = -(\phi + \theta)$ (in the first term). The modulation of the PB phase and propagation phase provides a useful method to tune the chiral optics as shown below.

(i) The case of $\theta + \phi = \pi$.

In this case, $H(\theta) = H(\phi)$. $(\mathbf{P}^A_L + e^{-ikz_0}\mathbf{P}^B_L)\cdot\hat{e}_R = (\mathbf{P}^A_R + e^{-ikz_0}\mathbf{P}^B_R)\cdot\hat{e}_L$. Under the additional condition of $z_0 = \lambda/2$, $(\mathbf{P}^A_L + e^{-ikz_0}\mathbf{P}^B_L)\cdot\hat{e}_L = (\mathbf{P}^A_R + e^{-ikz_0}\mathbf{P}^B_R)\cdot\hat{e}_R$. Then identical transmittances for LCP and RCP light for all $\theta = \pi - \phi$ are obtained, which has been verified by FDTD simulation (not shown here).

We then discuss LR and the related Wood's anomaly. From Eqs. (3) and (19), one can see that the quadratic terms of $\hat{\mathcal{G}}^{AA}_{xx}$ or $\hat{\mathcal{G}}^{AA}_{yy}$ in the denominator of $(\mathbf{P}_L, \mathbf{P}_R)$ are zero. So the denominator and numerator only have linear terms of $\hat{\mathcal{G}}^{AA}_{xx}$ and $\hat{\mathcal{G}}^{AA}_{yy}$. If $k = |\mathbf{L}_{(\pm1,0)}|$, only $\hat{\mathcal{G}}^{AA}_{yy}$ is divergent. In general, the divergent terms in the denominator and numerator cancel each other out ("∞/∞"), leading to the disappearance of Wood's anomaly as seen in Figs. 4(a) and 4(c). Compared with the results of monolayer as shown in Fig. 3, the interlayer coupling generally destroys the Wood's anomaly and related transparency, while in some specific conditions, the divergent terms in the numerator may be cancelled by the phase modulation. The coefficient $\hat{\mathcal{G}}^{AA}_{yy}$ in numerator for LCP(+) and RCP(−) is

$$e^{i(kz_0\pm\phi)}\sin\theta\sin\phi - e^{\pm i\theta}\sin^2\phi. \quad (21)$$

Under the condition $\theta = \pi - \phi = (\pi \pm kz_0)/2$, the above coefficient for LCP or RCP (not both) vanishes, which leads to the recovery of the transparency induced by Wood's anomaly for one of the circularly polarized lights. It is the chirality-selective transparency as seen in Fig. 4 (for $\theta = \pi/6$, $\phi = 5\pi/6$, and $z_0 = 200$ nm satisfying the condition). This transparency is obtained by modulating the PB phase and propagation phase [see Eq. (19)]. The nice agreement between the results from FDTD and CDM further verifies the analysis based on CDM.

From Eq. (21), one sees that the condition for chirality-selective transparency depends on the geometric parameters such as the twist angle and the separation between the nanorods. The phase-modulated lattice resonance and related chirality-selective transparency are the general effect. Changing the dimer length or the refractive index of the surrounding medium leads to a shift of the frequency of the LSPR of a single ellipsoid. The main physics of chirality-selective transparency remains unchanged.

(ii) The case of $\phi - \theta = \pi/2$.

It is known that a single nanorod dimer with twist angle $\pi/2$ possesses mirror symmetry; therefore, its CD is zero [52,55]. The collective effect in the dimer arrays leads to quite different chiral optical response. As seen in Figs. 5(a) and 5(b), the metasurfaces show different responses to LCP and RCP light. In general, the difference between the responses of LCP and RCP light is small due to the achiral nature of the unit cell. Actually, the difference vanishes for the square lattice as shown later. Here the dips are mainly contributed by LSPRs. For the case shown in Fig. 5(a), where the condition of chirality-selective transparency is satisfied, the metasurface shows significant difference of transmission for LCP and RCP light. In particular, the metasurface is transparent, "invisible" for RCP light with wavelength of 600 nm. Also the rods' long-axis dipole resonances disappear, and a weak electric field enhancement is observed in the electric field distribution shown in Figs. 5(e) and 5(f). Much stronger electric field enhancement is obtained for the LCP light (without transparency), and long-axis dipole resonances can be clearly seen in Figs. 5(c) and 5(d). The chiral response can be characterized by the g-factor as shown in Fig. 5(g). The FDTD simulation gives an absorption g-factor of 1.99 at wavelength of 600 nm (very close to the upper limit value of 2 due to the transparency). Figure 5(h) shows the chirality-selective transparency for metasurfaces with nanorods of different length, since the condition for chirality-selective transparency is independent of the length of the nanorods as seen from Eq. (21). In general, the LSPR wavelength shifts with changing the length of the nanorods. The resonant absorption of nanorods with long-axis radius of 82.5 nm occurs at a wavelength around 600 nm, leading to very small transmittance at a wavelength of 600 nm for LCP light.

In general, the phase states of transmission/reflection field depend on the detailed geometric parameters and wavelength, and the transmission and reflection waves are elliptically polarized. Using Eqs. (3), (10), and (12), one can see that at the lattice resonance ($\lambda = 600$ nm), transmission and reflection waves are circularly polarized with equal electric field amplitude in the x/y direction for transmitted and reflected far fields. For the RCP incident field, transparency appears, and the transmitted wave possesses phase difference (phase of the electric field in the x direction minus that in the y direction) $\pi/2$. For the LCP incident field, the transmission and reflection waves possess phase difference $-\pi/2$ and $\pi/2$.

2. Higher-Order Lattice Resonance

Similar discussion indicates that the mechanism of chirality-selective transparency also works for higher-order lattice resonances under the conditions of $k = |\mathbf{L}_{(\pm n,0)}|$ or $k = |\mathbf{L}_{(0,\pm n)}|$. An example, the transmittance of a metasurface under the condition $k = |\mathbf{L}_{(\pm 2,0)}|$ is displayed in Fig. 6(a).

The conditions for the chirality-selective transparency related to higher-order lattice resonance ($k = |\mathbf{L}_{(0,\pm n)}|$) are

$$e^{i(kz_0\pm\phi)}\cos\theta\cos\phi - e^{\pm i\theta}\cos^2\phi = 0, \quad (22)$$

which leads to $\theta = \pi - \phi = \pm kz_0/2$.

Here we would like to point out that the chirality-selective transparency associated with $k = |\mathbf{L}_{(\pm n,\pm m)}|$ $(n, m \neq 0)$ is absent. Unlike the cases of LR under the conditions $(k = |\mathbf{L}_{(\pm n,0)}|)/(k = |\mathbf{L}_{(0,\pm n)}|)$, both $\hat{\mathcal{G}}^{AA}_{xx}$ and $\hat{\mathcal{G}}^{AA}_{yy}$ are divergent for $k = |\mathbf{L}_{(\pm n,\pm m)}|$ $(n, m \neq 0)$. The coefficient of the term $(\hat{\mathcal{G}}^{AA}_{xx}\hat{\mathcal{G}}^{AA}_{yy}, \hat{\mathcal{G}}^{AB}_{xx}\hat{\mathcal{G}}^{AB}_{yy})$ in the denominator is

$$2\cos\theta\cos\phi\sin\theta\sin\phi - (\cos^2\theta\sin^2\phi + \cos^2\phi\sin^2\theta), \quad (23)$$

which is zero only for $\theta = \phi$. If $\theta \neq \phi$, the transparency associated with Wood's anomaly appears for LCP/RCP light as shown in Fig. 6(b). If $\theta = \phi$, the metasurface shows an achiral response. The small dip/peak at 465.5 nm in Fig. 6(b) is LR with $k = |\mathbf{L}_{(\pm 2,0)}|$. This wavelength is far from that for local plasmonic resonance, so the energy transmitted is very large. Because Eq. (21) is not satisfied, 100% transparency cannot be achieved.

3. Bilayer Metasurface with Square Lattice

The metasurface with a square lattice ($\Lambda_x = \Lambda_y$) possesses higher lattice symmetry than that with a rectangular lattice, which brings about new/different features in optical response. For the metasurface with a square lattice, $\hat{\mathcal{G}}^{AA}_{xx} = \hat{\mathcal{G}}^{AA}_{yy}$ and $\hat{\mathcal{G}}^{AB}_{xx} = \hat{\mathcal{G}}^{AB}_{yy}$, and the effective dipole moments are

$$\mathbf{p}^A_{L/R} = \frac{\sqrt{2}}{2}\frac{e^{i(kz_0\pm\phi)}\hat{\mathcal{G}}^{AB}_{xx}\cos(\theta-\phi) + e^{\pm i\theta}\left(\frac{1}{\alpha} - \hat{\mathcal{G}}^{AA}_{xx}\right)}{\left(\frac{1}{\alpha} - \hat{\mathcal{G}}^{AA}_{xx}\right)^2 - [\hat{\mathcal{G}}^{AB}_{xx}\cos(\theta-\phi)]^2}E_0\hat{e}_A,$$

$$\mathbf{p}^B_{L/R} = \frac{\sqrt{2}}{2}\frac{e^{\pm i\theta}\hat{\mathcal{G}}^{AB}_{xx}\cos(\theta-\phi) + e^{i(kz_0\pm\phi)}\left(\frac{1}{\alpha} - \hat{\mathcal{G}}^{AA}_{xx}\right)}{\left(\frac{1}{\alpha} - \hat{\mathcal{G}}^{AA}_{xx}\right)^2 - [\hat{\mathcal{G}}^{AB}_{xx}\cos(\theta-\phi)]^2}E_0\hat{e}_B. \quad (24)$$

There is no chirality-selective transparency because the necessary condition of transparency $\theta = \phi$ eliminates the chirality of the structure.

In the following, we consider the case of $\phi - \theta = \pi/2$. The term $H_{12} = \hat{\mathcal{G}}^{AB}_{xx}\cos(\theta - \phi)$ vanishes, indicating the effective decoupling of the upper and lower metasurfaces. Therefore, the

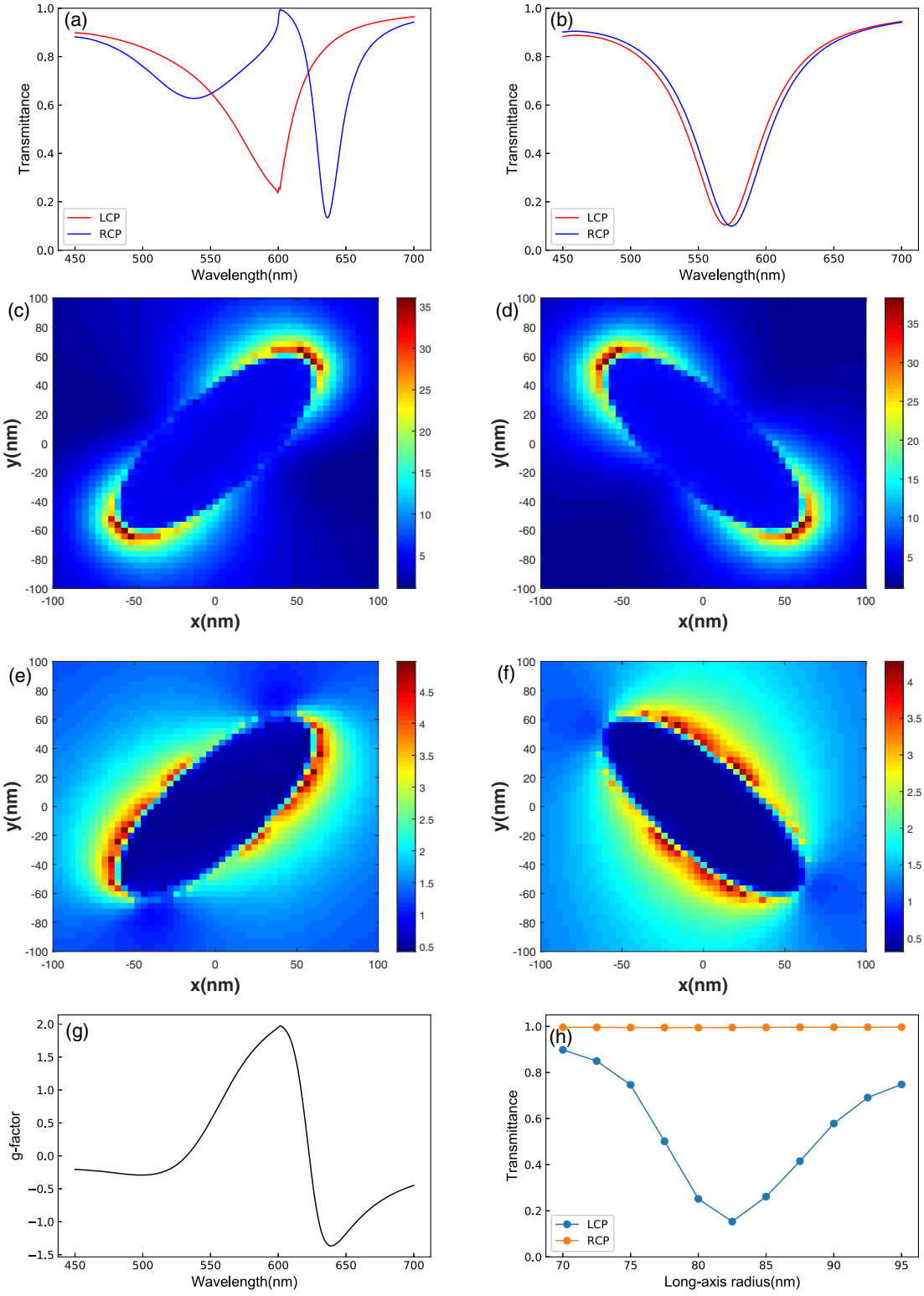

Fig. 5. (a), (b) Transmittance of a metasurface with achiral building blocks [i.e., unit cell with nanorod dimer of twist angle $\pi/2$ ($\theta = \pi/4$ and $\phi = 3\pi/4$)] based on FDTD simulation. (a) $\Lambda_x = 600$ nm, $\Lambda_y = 350$ nm, $z_0 = 150$ nm (the condition of chirality-selective transparency is satisfied); (b) $\Lambda_x = 400$ nm, $\Lambda_y = 350$ nm, $z_0 = 150$ nm (the condition of chirality-selective transparency is violated). (c)–(f) The electric field distribution ($|\boldsymbol{E}|$) for nanorods A and B at wavelength of 600 nm. (c), (d) The distribution at the x–y cross-section plane with $z = 0$ (rod A)/150 nm (rod B) for LCP light; (e), (f) the distribution at the x–y cross-section plane with $z = 0/150$ nm for RCP light. The other parameters are the same as those in (a). (g) The g-factor corresponding to (a). (h) The transmittance versus the long-axis radius of the nanorods at a wavelength of 600 nm.

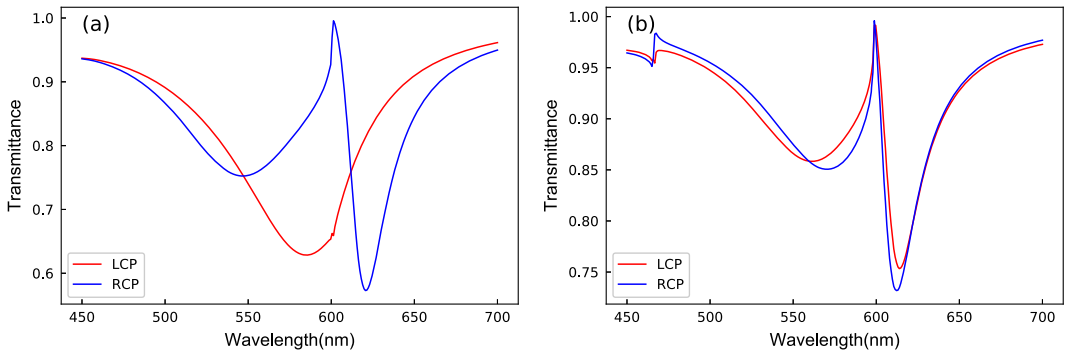

Fig. 6. Transmittance of LCP/RCP light associated with higher-order resonance based on FDTD simulation. (a) $\theta = \pi/4$, $\phi = 3\pi/4$, $\Lambda_x = 1200$ nm and $\Lambda_y = 300$ nm, $z_0 = 150$ nm. $k = |\mathbf{L}_{(\pm 2,0)}|$. (b) $\theta = \pi/4$, $\phi = 3\pi/4$, $\Lambda_x = 931$ nm and $\Lambda_y = 781$ nm, $z_0 = 150$ nm. $k = |\mathbf{L}_{(\pm 1,\pm 1)}|$.

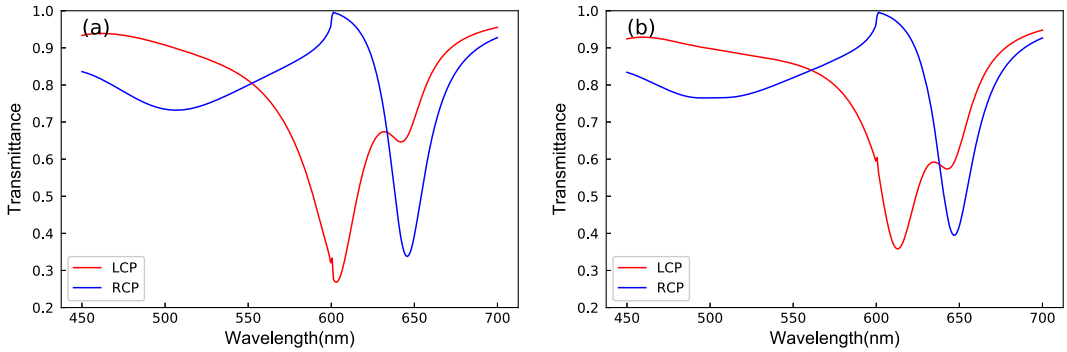

Fig. 7. Transmittance of LCP/RCP light with $\Lambda_x = 600$ nm and $\Lambda_y = 350$ nm calculated by the FDTD method. (a) $z_0 = 90$ nm, $\theta = 7\pi/20$, and $\phi = 13\pi/20$. (b) $z_0 = 75$ nm, $\theta = 3\pi/8$, and $\phi = 5\pi/8$.

bilayer metasurface shows achiral optical response like that of the monolayer metasurface. Also, the transparency due to Wood's anomaly appears for both LCP and RCP light. From Eq. (24), we find that the scattering far field $\mathbf{E}^{\text{far}}_{L/R} \propto \mathbf{P}^{A}_{L/R} + e^{-ikz_0}\mathbf{P}^{B}_{L/R} \propto \frac{1}{H}\hat{e}_{L/R}$, with H independent of θ or ϕ. In general, for the metasurface with a rectangular lattice in the presence of normally incident LCP/RCP field, the transmitted field contains both LCP and RCP components [see Eq. (19)]. For the metasurface with a square lattice in the presence of normally incident LCP/RCP field, the transmitted field contains only an LCP/RCP component. Moreover, the transmittance is independent of θ or ϕ.

4. Beyond Coupled Dipole Approximation

The above analytical calculations are based on CDM. The interparticle distances are chosen to be larger than 3 times the radius in the transverse direction to ensure the validity of coupled dipole approximation, which has also been verified by the FDTD simulations. We would like to note that some of the results can be extended to the parameter range beyond the coupled dipole approximation. The transmission spectra for the cases with smaller interparticle distance are shown in Figs. 7(a) and 7(b), where gaps between the surfaces of the upper and lower layers are 30 nm and 15 nm. Here our FDTD calculations show that the chirality-selective transparency still exists under the condition of Eq. (21).

4. CONCLUSION

We theoretically explore the chiral optics of bilayer metasurfaces made of twisted nanorods, focusing on the collective effect due to LR. Through detailed analytical calculation based on CDM and FDTD simulations, we find that combination effects from LR and phase modulation (PB phase, propagation phase) can bring about novel chiral optical responses, including chirality-selective transparency (recovery of Wood's anomaly) and chiral response for metasurfaces with achiral unit cells. The theoretical results deepen our understanding of light–matter interaction at the nanometer scale. In particular, the analytical results (supported by numerical simulation) give a quantitative relationship between local geometric structure, lattice structure, and their (chiral) optical properties; for example, the condition for chirality-selective transparency $\theta = \pi - \phi = \frac{\pi \pm kz_0}{2}$. Those special properties of metasurfaces could play important roles in optical communication, circular dichroism spectroscopy, and quantum information processing.

Funding. National Key Research and Development Program of China (2017YFA0303400); National Natural Science Foundation of China-Research Grants Council (11861161002); National Natural Science Foundation of China (11774036).

Disclosures. The authors declare no conflicts of interest.

REFERENCES

1. F. J. García de Abajo, "Colloquium: light scattering by particle and hole arrays," Rev. Mod. Phys. **79**, 1267–1290 (2007).
2. Z. Fan and A. O. Govorov, "Plasmonic circular dichroism of chiral metal nanoparticle assemblies," Nano Lett. **10**, 2580–2587 (2010).
3. A. Kuzyk, R. Schreiber, Z. Fan, G. Pardatscher, E.-M. Roller, A. Högele, F. C. Simmel, A. O. Govorov, and T. Liedl, "DNA-based self-assembly of chiral plasmonic nanostructures with tailored optical response," Nature **483**, 311–314 (2012).
4. V. E. Ferry, J. M. Smith, and A. P. Alivisatos, "Symmetry breaking in tetrahedral chiral plasmonic nanoparticle assemblies," ACS Photon. **1**, 1189–1196 (2014).
5. M. Hentschel, V. E. Ferry, and A. P. Alivisatos, "Optical rotation reversal in the optical response of chiral plasmonic nanosystems: the role of plasmon hybridization," ACS Photon. **2**, 1253–1259 (2015).
6. N. Liu and H. Giessen, "Coupling effects in optical metamaterials," Angew. Chem. **49**, 9838–9852 (2010).
7. W. Ma, F. Cheng, and Y. Liu, "Deep-learning-enabled on-demand design of chiral metamaterials," ACS Nano **12**, 6326–6334 (2018).
8. C. Shen, X. Lan, C. Zhu, W. Zhang, L. Wang, and Q. Wang, "Spiral patterning of Au nanoparticles on Au nanorod surface to form chiral AuNR@AuNP helical superstructures templated by DNA origami," Adv. Mater. **29**, 1606533 (2017).
9. B. Auguié, J. L. Alonso-Gómez, A. Guerrero-Martínez, and L. M. Liz-Marzán, "Fingers crossed: optical activity of a chiral dimer of plasmonic nanorods," J. Phys. Chem. Lett. **2**, 846–851 (2011).
10. X. Yin, M. Schäferling, B. Metzger, and H. Giessen, "Interpreting chiral nanophotonic spectra: the plasmonic Born–Kuhn model," Nano Lett. **13**, 6238–6243 (2013).
11. L.-Y. Wang, K. W. Smith, S. Dominguez-Medina, N. Moody, J. M. Olson, H. Zhang, W.-S. Chang, N. Kotov, and S. Link, "Circular differential scattering of single chiral self-assembled gold nanorod dimers," ACS Photon. **2**, 1602–1610 (2015).
12. X. Yin, M. Schäferling, A.-K. U. Michel, A. Tittl, M. Wuttig, T. Taubner, and H. Giessen, "Active chiral plasmonics," Nano Lett. **15**, 4255–4260 (2015).
13. C. Rao, Z.-G. Wang, N. Li, W. Zhang, X. Xu, and B. Ding, "Tunable optical activity of plasmonic dimers assembled by DNA origami," Nanoscale **7**, 9147–9152 (2015).
14. A. F. Najafabadi and T. Pakizeh, "Analytical chiroptics of 2D and 3D nanoantennas," ACS Photon. **4**, 1447–1452 (2017).
15. M. Hentschel, M. Schäferling, X. Duan, H. Giessen, and N. Liu, "Chiral plasmonics," Sci. Adv. **3**, e1602735 (2017).
16. M. J. Urban, C. Shen, X.-T. Kong, C. Zhu, A. O. Govorov, Q. Wang, M. Hentschel, and N. Liu, "Chiral plasmonic nanostructures enabled by bottom-up approaches," Annu. Rev. Phys. Chem. **70**, 275–299 (2019).
17. A. Christofi, N. Stefanou, G. Gantzounis, and N. Papanikolaou, "Giant optical activity of helical architectures of plasmonic nanorods," J. Phys. Chem. C **116**, 16674–16679 (2012).
18. A. Christofi, N. Stefanou, G. Gantzounis, and N. Papanikolaou, "Spiral-staircase photonic structures of metallic nanorods," Phys. Rev. B **84**, 125109 (2011).
19. Y. Zhao, M. Belkin, and A. Alù, "Twisted optical metamaterials for planarized ultrathin broadband circular polarizers," Nat. Commun. **3**, 870 (2012).
20. A. N. Askarpour, Y. Zhao, and A. Alù, "Wave propagation in twisted metamaterials," Phys. Rev. B **90**, 054305 (2014).
21. Y. Cui, L. Kang, S. Lan, S. Rodrigues, and W. Cai, "Giant chiral optical response from a twisted-arc metamaterial," Nano Lett. **14**, 1021–1025 (2014).
22. B. Hopkins, A. N. Poddubny, A. E. Miroshnichenko, and Y. S. Kivshar, "Circular dichroism induced by Fano resonances in planar chiral oligomers," Laser Photon. Rev. **10**, 137–146 (2016).
23. S. Fasold, S. Linß, T. Kawde, M. Falkner, M. Decker, T. Pertsch, and I. Staude, "Disorder-enabled pure chirality in bilayer plasmonic metasurfaces," ACS Photon. **5**, 1773–1778 (2018).
24. J. K. Gansel, M. Thiel, M. S. Rill, M. Decker, K. Bade, V. Saile, G. von Freymann, S. Linden, and M. Wegener, "Gold helix photonic metamaterial as broadband circular polarizer," Science **325**, 1513–1515 (2009).
25. S. Yang, Z. Liu, S. Hu, A.-Z. Jin, H. Yang, S. Zhang, J. Li, and C. Gu, "Spin-selective transmission in chiral folded metasurfaces," Nano Lett. **19**, 3432–3439 (2019).
26. S. Yang, Z. Liu, H. Yang, A. Jin, S. Zhang, J. Li, and C. Gu, "Intrinsic chirality and multispectral spin-selective transmission in folded eta-shaped metamaterials," Adv. Opt. Mater. **8**, 1901448 (2019).
27. V. A. Fedotov, P. L. Mladyonov, S. L. Prosvirnin, A. V. Rogacheva, Y. Chen, and N. I. Zheludev, "Asymmetric propagation of electromagnetic waves through a planar chiral structure," Phys. Rev. Lett. **97**, 167401 (2006).
28. V. A. Fedotov, A. S. Schwanecke, N. I. Zheludev, V. V. Khardikov, and S. L. Prosvirnin, "Asymmetric transmission of light and enantiomerically sensitive plasmon resonance in planar chiral nanostructures," Nano Lett. **7**, 1996–1999 (2007).
29. C. Menzel, C. Helgert, C. Rockstuhl, E.-B. Kley, A. Tünnermann, T. Pertsch, and F. Lederer, "Asymmetric transmission of linearly polarized light at optical metamaterials," Phys. Rev. Lett. **104**, 253902 (2010).
30. P. Yu, J. Li, C. Tang, H. Cheng, Z. Liu, Z. Li, Z. Liu, C. Gu, J. Li, S. Chen, and J. Tian, "Controllable optical activity with non-chiral plasmonic metasurfaces," Light Sci. Appl. **5**, e16096 (2016).
31. L. Huang, X. Chen, H. Mühlenbernd, G. Li, B. Bai, Q. Tan, G. Jin, T. Zentgraf, and S. Zhang, "Dispersionless phase discontinuities for controlling light propagation," Nano Lett. **12**, 5750–5755 (2012).
32. B. Bai, Y. Svirko, J. Turunen, and T. Vallius, "Optical activity in planar chiral metamaterials: theoretical study," Phys. Rev. A **76**, 023811 (2007).
33. X. Chen, L. Huang, H. Mühlenbernd, G. Li, B. Bai, Q. Tan, G. Jin, C.-W. Qiu, S. Zhang, and T. Zentgraf, "Dual-polarity plasmonic metalens for visible light," Nat. Commun. **3**, 1198 (2012).
34. N. Yu, P. Genevet, M. A. Kats, F. Aieta, J.-P. Tetienne, F. Capasso, and Z. Gaburro, "Light propagation with phase discontinuities: generalized laws of reflection and refraction," Science **334**, 333–337 (2011).
35. J. Sperrhake, M. Decker, M. Falkner, S. Fasold, T. Kaiser, I. Staude, and T. Pertsch, "Analyzing the polarization response of a chiral metasurface stack by semi-analytic modeling," Opt. Express **27**, 1236–1248 (2019).
36. T. Paul, C. Menzel, W. Śmigaj, C. Rockstuhl, P. Lalanne, and F. Lederer, "Reflection and transmission of light at periodic layered metamaterial films," Phys. Rev. B **84**, 115142 (2011).
37. Y. Tang and A. E. Cohen, "Optical chirality and its interaction with matter," Phys. Rev. Lett. **104**, 163901 (2010).
38. Y. Tang and A. E. Cohen, "Enhanced enantioselectivity in excitation of chiral molecules by superchiral light," Science **332**, 333–336 (2011).
39. J. Lasa-Alonso, D. R. Abujetas, A. Nodar, J. A. Dionne, J. J. Saenz, G. Molina-Terriza, J. Aizpurua, and A. Garcia-Etxarri, "Surface-enhanced circular dichroism spectroscopy on periodic dual nanostructures," ACS Photon. **7**, 2978–2986 (2020).
40. A. F. Koenderink and A. Polman, "Complex response and polariton-like dispersion splitting in periodic metal nanoparticle chains," Phys. Rev. B **74**, 033402 (2006).
41. P. Lunnemann, I. Sersic, and A. F. Koenderink, "Optical properties of two-dimensional magnetoelectric point scattering lattices," Phys. Rev. B **88**, 245109 (2013).
42. A. Kwadrin and A. F. Koenderink, "Diffractive stacks of metamaterial lattices with a complex unit cell: self-consistent long-range bianisotropic interactions in experiment and theory," Phys. Rev. B **89**, 045120 (2014).
43. M. Cotrufo, C. I. Osorio, and A. F. Koenderink, "Spin-dependent emission from arrays of planar chiral nanoantennas due to lattice and localized plasmon resonances," ACS Nano **10**, 3389–3397 (2016).
44. S. Baur, S. Sanders, and A. Manjavacas, "Hybridization of lattice resonances," ACS Nano **12**, 1618–1629 (2018).

45. D. DeJarnette, J. Norman, and D. K. Roper, "Attribution of Fano resonant features to plasmonic particle size, lattice constant, and dielectric wavenumber in square nanoparticle lattices," Photon. Res. **2**, 15–23 (2014).
46. S. Zu, Y. Bao, and Z. Fang, "Planar plasmonic chiral nanostructures," Nanoscale **8**, 3900–3905 (2016).
47. Y. Hwang, S. Lee, S. Kim, J. Lin, and X.-C. Yuan, "Effects of Fano resonance on optical chirality of planar plasmonic nanodevices," ACS Photon. **5**, 4538–4544 (2018).
48. Y. Hwang, B. Hopkins, D. Wang, A. Mitchell, T. J. Davis, J. Lin, and X.-C. Yuan, "Optical chirality from dark-field illumination of planar plasmonic," Laser Photon. Rev. **11**, 1700216 (2017).
49. Z. Liu, Y. Xu, C.-Y. Ji, S. Chen, X. Li, X. Zhang, Y. Yao, and J. Li, "Fano-enhanced circular dichroism in deformable stereo metasurfaces," Adv. Mater. **32**, 1907077 (2020).
50. S.-D. Liu, J.-Y. Liu, Z. Cao, J.-L. Fan, and D. Lei, "Dynamic tuning of enhanced intrinsic circular dichroism in plasmonic stereo-metamolecule array with surface lattice resonance," Nanophotonics **9**, 3419–3434 (2020).
51. E. S. A. Goerlitzer, R. Mohammadi, S. Nechayev, K. Volk, M. Rey, P. Banzer, M. Karg, and N. Vogel, "Chiral surface lattice resonances," Adv. Mater. **32**, 2001330 (2020).
52. S.-X. Zhao and W. Zhang, "Plasmonic chirality of one-dimensional arrays of twisted nanorod dimers: the cooperation of local structure and collective effect," Opt. Express **27**, 38614–38623 (2019).
53. Z. Bomzon, G. Biener, V. Kleiner, and E. Hasman, "Space-variant Pancharatnam–Berry phase optical elements with computer-generated subwavelength gratings," Opt. Lett. **27**, 1141–1143 (2002).
54. G. Milione, S. Evans, D. A. Nolan, and R. R. Alfano, "Higher order Pancharatnam-Berry phase and the angular momentum of light," Phys. Rev. Lett. **108**, 190401 (2012).
55. W. Zhang, *Chirality at Nanoscale-Theory and Mechanism in Chiral Nanomaterials: Preparation, Properties and Applications*, Z. Tang, ed. (Wiley, 2018).
56. A. B. Evlyukhin, C. Reinhardt, A. Seidel, B. S. Luk'yanchuk, and B. N. Chichkov, "Optical response features of Si-nanoparticle arrays," Phys. Rev. B **82**, 045404 (2010).
57. S. A. Maier, *Plasmonics: Fundamentals and Applications* (Springer, 2007).
58. H. Kuwata, H. Tamaru, K. Esumi, and K. Miyano, "Resonant light scattering from metal nanoparticles: practical analysis beyond Rayleigh approximation," Appl. Phys. Lett. **83**, 4625–4627 (2003).
59. A. B. Evlyukhin, C. Reinhardt, and B. N. Chichkov, "Multipole light scattering by nonspherical nanoparticles in the discrete dipole approximation," Phys. Rev. B **84**, 235429 (2011).
60. A. B. Evlyukhin, C. Reinhardt, E. Evlyukhin, and B. N. Chichkov, "Multipole analysis of light scattering by arbitrary-shaped nanoparticles on a plane surface," J. Opt. Soc. Am. B **30**, 2589–2598 (2013).
61. A. B. Evlyukhin, T. Fischer, C. Reinhardt, and B. N. Chichkov, "Optical theorem and multipole scattering of light by arbitrarily shaped nanoparticles," Phys. Rev. B **94**, 205434 (2016).
62. E. D. Palik, *Handbook of Optical Constants of Solids* (Academic, 1998).
63. B. Auguié and W. L. Barnes, "Collective resonances in gold nanoparticle arrays," Phys. Rev. Lett. **101**, 143902 (2008).